Numerical Modelling of Solar Receivers Equipped With TPMS Structures

SolarPACES 2024, 30th International Conference on Concentrating Solar Power, Thermal, and Chemical Energy Systems

Receivers and Heat Transfer Media and Transport: Linear Systems

https://doi.org/10.52825/solarpaces.v3i.2416

Published: 25 Nov. 2025

Numerical Modelling of Solar Receivers Equipped With TPMS Structures

Arsham Mortazavi[1], Hossein Ebadi[1], Cecilia Piatti[1], Eleonora Gajetti[1], Luca Marocco[2], and Laura Savoldi[3,*]

[1]Politecnico di Torino, Italy

[2]Politecnico di Milano, Italy

*Correspondence: Laura Savoldi, laura.savoldi@polito.it

Abstract. In this study, two planar high-temperature solar receivers, equipped with Triply Periodic Minimal Surface lattices of Diamond and SplitP, were analysed numerically. These receivers were manufactured and experimentally tested in a previous study. Different RANS turbulence models, including Lag EB κ-ε, κ-ω SST (Menter), and Realizable κ-ε two-layer, were evaluated, and their results were compared with experimental data. A comprehensive validation revealed that the Lag EB κ-ε and κ-ω SST (Menter) models have the smallest deviation from the experimental data. The sample with the SplitP lattice demonstrated superior thermal performance with higher thermal efficiency, higher useful heat, and exhibiting a slightly lower maximum surface temperature and a narrower high-temperature region.

Keywords: TPMS, CFD, CSP

1. Introduction

Concentrated solar power (CSP) plants are increasingly relevant for renewable energy, and advancing to cheaper heat transfer fluids (HTF), such as air, is a promising option, despite the lower heat transfer capacity compared to current molten salt and thermal oil options. To enhance the receiver performance, different thermal enhancement devices and configurations are under considerations.

Triply Periodic Minimal Surfaces (TPMS) are a promising class of geometric structures, that recently gained an increasing interest in various engineering applications, especially heat exchangers [1]. TPMS structures exhibit three-dimensional periodicity and minimal surfaces with a high surface area-to-volume ratio, making them ideal for enhancing heat transfer efficiency while maintaining a low pressure drop [2]. The practical application of TPMS in engineering has only recently gained attention due to advancements in Additive Manufacturing (AM), which allows for the creation of these structures through 3D printing. Considering heat management and energy systems, TPMS have significantly advanced current technologies in a wide range of energy applications. Dutkowski et al. [3] provided a state-of-the-art review of minimal surfaces in heat transfer, emphasizing the potential of TPMS as a promising surface type for heat exchangers. However, TPMS application in solar energy systems remains relatively rare and is still in its early stages, and only recently numerical assessments have demonstrated the potential of TPMS for solar thermal applications, particularly as volumetric receivers [4, 5]. Mortazavi et al. [6] conducted an experimental test campaign to explore the energy and exergy efficiency of two TPMS-based planar samples for application as high-temperature solar

receivers. The two stainless samples equipped with SplitP, and Diamond lattices were fabricated using AM, and tested in a solar simulator. Results indicated that the sample with SplitP lattice outperforms the one with Diamond lattice.

Although the published experimental results have demonstrated the applicability of TPMS structures for air-based solar receivers, there is a lack of numerical studies addressing real-scale solar simulations of such absorbers. This gap in the literature hinders designers and engineers from fully understanding the heat transfer mechanisms involved and then proceed to the optimization of the receiver. As a result, this study aims at developing a 3D CFD model for the samples tested in Ref. [6], simulating TPMS-based CSP receivers under real-scale conditions to provide further insights on the performance of these receivers. The impact of different turbulence models is considered, in the comparison to experimental data for both the lattices for which experimental data are available (i.e., Diamond and SplitP).

This paper is organized as follows: Section 0 presents a brief description of the modelled receiver, the experimental tests conducted, the inputs used in numerical simulations, and a sensitivity analysis of the grid network developed for the solution domain. Section 0 discusses the validation of the developed numerical model against experimental results, explaining how numerical factors such as turbulence models could affect the accuracy of the model predictions. Section 0 provides additional thermal analyses, detailing the temperature distribution and hotspot regions of the receivers. Finally, the conclusions are summarized in Section 0.

2. Methodology

2.1 Solar receivers and experimental campaign

The small-scale planar solar receivers were designed and manufactured in AISI 316L as shown in *Figure 1*a-b. Experiments were conducted at IMDEA Energy, Madrid (Spain) in the KIRAN-42 high-flux solar simulator, with a total radiation power of 14 kW with a peak heat focal plane [7]. Synthetic air, composed of 79% nitrogen and 21% oxygen, at ~10 bar was used as HTF. Inlet and outlet temperatures, as well as absolute pressures, were measured before and after the sample. The temperature of the backside and bottom-side of the samples was measured using four thermocouples, with their locations on the mounted sample shown in *Figure 1*c. A series of experimental tests, studying the effects of airflow rate and solar heat flux were investigated for each sample. The test conditions of the present work are based on the heat flux level of 200 kW/m^2 tested under different airflow rates (see *Table 1*). Note that, due to the negligible pressure drops across the samples (below the uncertainty of the pressure gauge), hydraulic measurements are not included in this study.

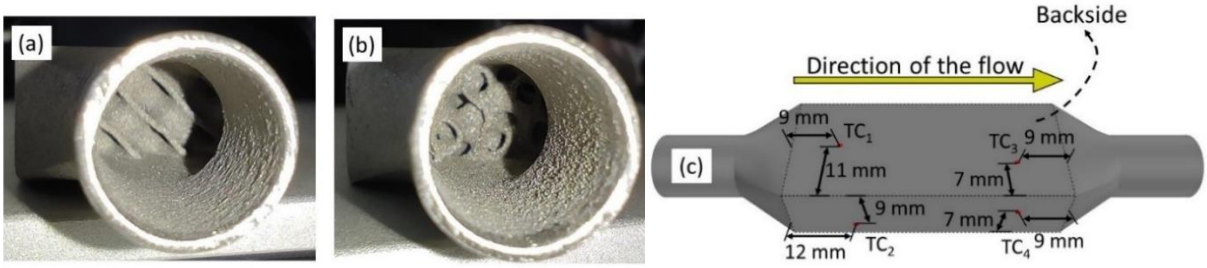

Figure 1. *Pictures of the manufactured samples with (a) Diamond lattice and (b) SplitP lattice, and (c) schematics of temperature sensors' locations.*

As in TPMS structures the cross-sectional area and the wetted perimeter could vary along their length, their hydraulic diameter is defined as a ratio between the volume of the fluid domain to the wetted surface (see Eq. 1).

$$D_h = \frac{4V_{fluid}}{A_{wet}} \quad (1)$$

The Reynolds number is defined based on hydraulic diameter in Eq. 2.

$$Re = \frac{\rho U D_h}{\mu} \quad (2)$$

U is the pore velocity and is equal to $\frac{\dot{m}}{A_c \varepsilon \rho}$, in which A_c is the cross-sectional area of the channel without the TPMS lattice. The Reynolds number corresponding to the mass flow rates varies between 430 to 1700 for the SplitP lattice, while it is between 530 to 2100 for the Diamond; therefore, the Reynolds number is well above the Darcy regime, suggesting that the flow is in its inertial regime.

Table 1. *Experimental test parameters measured during the campaign and used for model development.*

Mass flow rate (g/s)	**Peak heat flux (kW/m²)**	**$\Delta T_{Diamond}$ ($T_{outlet} - T_{inlet}$) (K)**	**ΔT_{SplitP} ($T_{outlet} - T_{inlet}$) (K)**
0.5	200	125	155
1	200	87	109
1.5	200	66	71
2	200	53	65

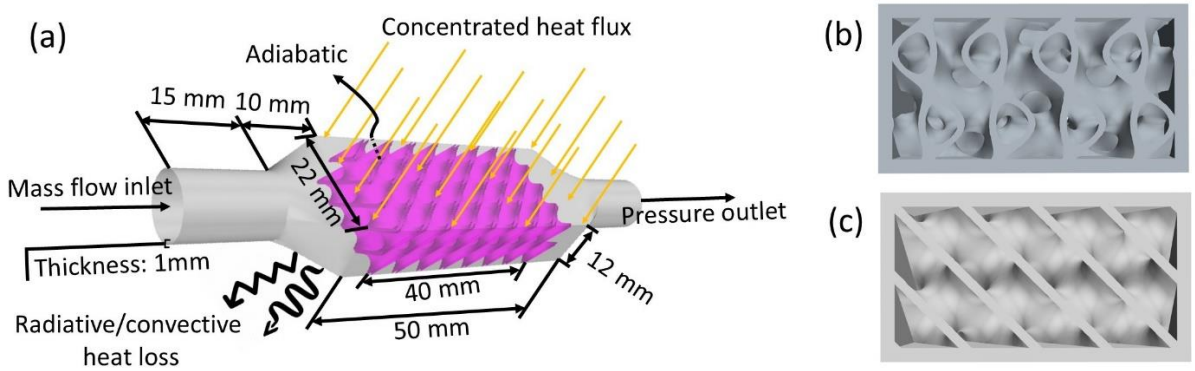

Figure 2*. Geometry and boundary conditions of the samples (Diamond sample); The sample with (a) SplitP and (b) Diamond lattice in a cross-section in the middle of the sample.*

A numerical 3D conjugate heat-transfer model was developed, using the STAR-CCM+ software for the samples with a non-uniform and one-side heating solar exposure, affected by the convection and radiation losses to the ambient. Different RANS turbulent models, and namely the Lag EB κ-ε, κ-ω SST (Menter) and Realizable κ-ε two-layer have been investigated.

The solar heat flux (Q_s) used as input in the simulations was modelled using a correlation (Eq. 3) derived from the best fit to experimental data along the x- and y-axes [6].

$$Q_s = A + He^{-0.5\left[\left(\frac{x}{\sigma_x}\right)^2 + \left(\frac{y}{\sigma_y}\right)^2\right]} \quad (3)$$

In Eq. 3, A = 94.43 kW/m², H = 245.08 kW/m² and $\sigma_x = \sigma_y = 15.575$ are the standard deviations in x and y directions. Radiative ($Q_{l,rad}$) and convective ($Q_{l,conv}$) heat loss rates were applied to all absorber surfaces except for the bottom-side surface. In the experiments, the bottom-side surface was covered by insulation to protect the thermocouples from being exposed to incident heat flux. As in the experiments the results were obtained after a quasi-steady state condition was met, the simulations were performed under steady state condition.

$$Q_{l,conv} = h\,(T_{abs} - T_{amb}) \tag{4}$$

$$Q_{l,rad} = \sigma \varepsilon_{abs} (T_{abs}^4 - T_{amb}^4) \tag{5}$$

In which h is the convective heat transfer coefficient assumed as 10 W/m^{2}K, σ is the Stefan Boltzmann constant, and ε_{abs} is the absorber emissivity. The surface of the receiver was assumed to be grey, so that $\varepsilon_{abs} = \alpha$. Moreover, T_{abs} and T_{amb} denote the temperature of the external wall of the absorber and the ambient temperatures. The useful heat, the amount of thermal energy transferred to the HTF, which is used to increase the air temperature, can be calculated from Eq. 6.

$$Q_{usf} = \alpha Q_s - (Q_{l,conv} + Q_{l,rad}) \tag{6}$$

where, α is the receiver absorptivity and implied the amount of heat absorbed by the samples. According to [8] the exposure of a stainless-steel solar absorber to high-flux solar incident radiation leads to oxidation, providing a shift into the surface optical properties. As already seen by Cantone et al. [9], for a similar heat flux range, oxidation occurs on the uncoated receivers. Boydağ [8] studied the optical properties of different stainless steels for high-temperature applications. The value of absorptivity used in this study was 0.59, obtained from Ref. [8] for almost the same level of oxidation and its validity was investigated in *Figure 3*. In this figure, the thermal efficiency of the numerical results was compared to experimental data indicating a good consistency. As in the experiments the useful heat was obtained from Eq. 7, the useful heat is evaluated in the simulations in the same way and double checked with Eq. 6.

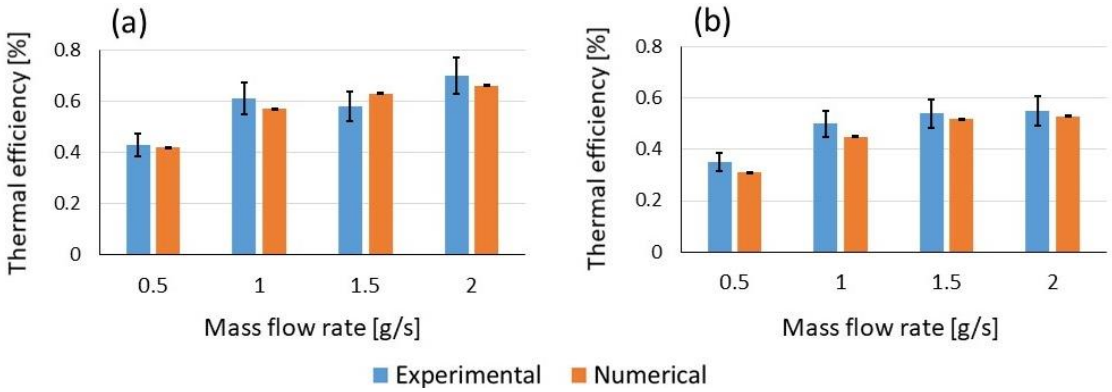

Figure 3. *Thermal efficiency comparison between experimental and numerical (from Lag EB κ-ε RANS model) results for different mass flow rates, heat flux level of 200 kW/m2 for (a) SplitP lattice (b) Diamond lattice.*

$$Q_{usf} = \dot{m} c_p (T_{m,outlet} - T_{inlet}) \tag{7}$$

In the simulations, the specific heat at constant pressure c_p, was obtained at the mean arithmetic temperature between inlet and outlet, while the air inlet and outlet temperatures are the adiabatic mean values. Finally, the thermal efficiency, which is the ratio between the useful heat (Q_{usf}) and the total solar incident radiation (Q_s) can be given with Eq. 8.

$$\eta_{th} = \frac{Q_{usf}}{Q_s} \tag{8}$$

The heat transfer fluid in the tests was synthetic air with 79% Nitrogen and 21% Oxygen. In the simulations, the non-reacting multi-component gas mixture, with the same composition of the experiments, was assumed to be an ideal gas with temperature-dependant properties.

2.2 Grid study

To solve the equations, polyhedral meshing was used with prismatic layers (for the fluid region) to well capture high temperature and velocity gradients in near wall regions. A comprehensive grid study was conducted to ascertain the accuracy of the results related to the discretization error. Four different grids were developed and simulated with different RANS models comparing the pressure drop and useful heat. In *Table 2*, grid study for Lag EB κ-ε RANS model could be seen. In this table, grid ID is named with the first letter of the lattice and starting from the finest to coarsest, e.g., S3 is the finest grid for SplitP while S0 is the coarsest one. In this table, r_{i3} is the ratio between the number of cells of the $i-th$ grid to the finest grid (grid number 3). To estimate the uncertainty of the results due to discretization error, Grid Convergence Index (GCI) was calculated using the least squares approach.

Table 2. *Grid study for Lag EB κ-ε RANS model.*

Grid ID	Number of cells	r_{i3}	Average cell size (Δh) [m]	$\Delta p / \Delta p_{finest}$	$Q_{useful} / Q_{useful,finest}$
S3	5.07E+06	1	1.59E-04	1.00	1.0000
S2	4.21E+06	0.849	1.69E-04	1.007	1.0003
S1	3.30E+06	0.668	1.83E-04	1.011	0.9983
S0	2.39E+06	0.484	2.04E-04	1.072	0.9985
D3	2.84E+06	1	1.92E-04	1.00	1.0000
D2	2.29E+06	0.830	2.07E-04	0.985	1.0003
D1	2.09E+06	0.760	2.13E-04	0.963	0.9992
D0	1.95E+06	0.713	2.07E-04	0.944	0.9977

3. Validation of the results

3.1 Effects of turbulence model

In **Figure 4**, Q_{usf} obtained from different RANS turbulent models is compared. For both samples, Lag EB κ-ε and κ-ω SST (Menter) models resulted in minimum deviation from the experimental results. In **Figure 4**, for almost all the mass flow rates the experimental data are higher than the corresponding numerical values. One reason for that could be the effect of surface roughness which is not considered in numerical simulations. In *Figure 1*a-b it is indeed evident that the surface of the manufactured samples are rather rough which leads to enhanced heat transfer between the absorber and HTF.

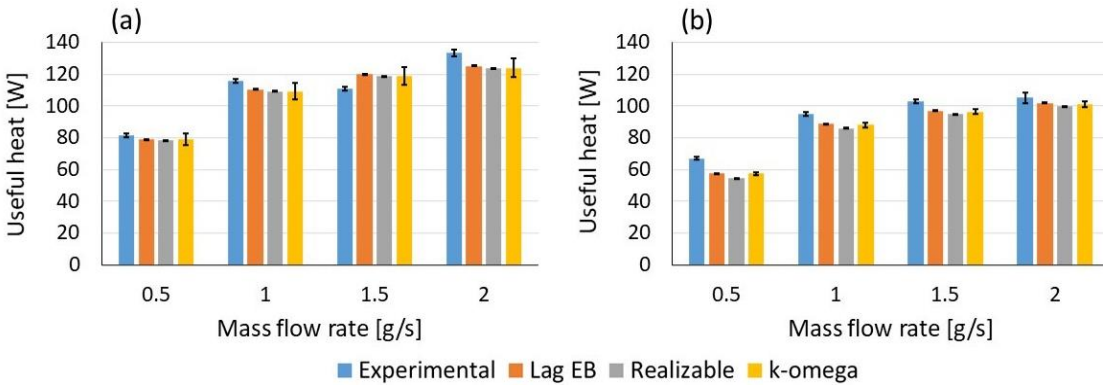

Figure 4. *Comparison of the results of different RANS models for (a) SplitP and (b) Diamond lattices.*

3.2 Validation on the wall temperature increases

To further validate the models, the wall temperature of the samples was compared with experimental data. The temperature increases of TC_2 and TC_4 (compared to inlet temperature) could be seen in *Figure 5*. TC_2 and TC_4 were selected because, in the experiments, they had better contact with the samples. They were secured using a screw-tightened clamp mechanism that held the Alumina insulation on the bottom side of the samples. *Figure 5* shows the good agreement between the results from the Lag EB κ-ε model and the experimental data.

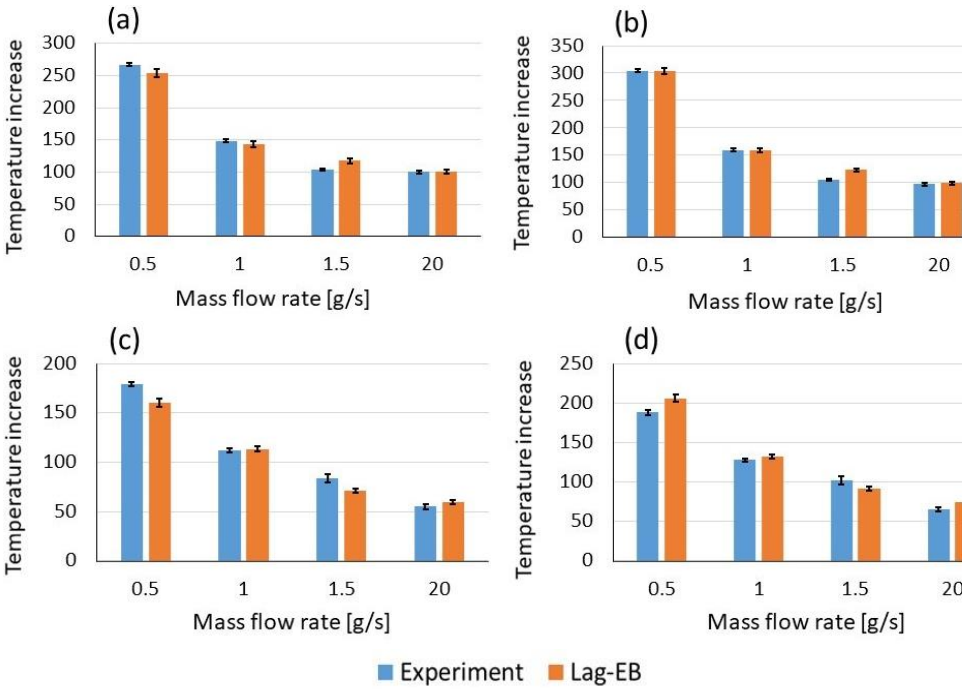

Figure 5. *Temperature increases in K (compared to inlet temperature) of the SplitP lattice for (a) TC_2 and (b) TC_4; temperature increase of the Diamond lattice for (c) TC_2 and (d) TC_4.*

4. Thermal analyses

The hotspot temperatures of the samples could be seen in **Figure 6**a. The temperature maps for the most critical mass flow rate (0.5 g/s) could be seen in **Figure 6**b-c. The hot spot is located near to the outlet with SplitP lattice having slightly smaller maximum temperature. From **Error! Reference source not found.**b, it appears that the high temperature values occupy a wider region for the Diamond lattice. The SplitP lattice has a higher effective conductivity compared to Diamond lattice (see [6]) which results in its superior heat removal effect. Beside this, higher thermal performance of SplitP lattice could also be attributed to its higher surface area-to-volume ratio (1.43 mm^{-1} and 1.06 mm^{-1} for SplitP and Diamond lattices, respectively) and its complex flow channels which lead to better mixing of the HTF.

In **Figure 7**, the useful heat predicted by the Lag EB κ-ε model is compared for the two lattices. The results align well with the experimental data, where the SplitP lattice sample showed higher absorbed heat (see Ref. [6]).

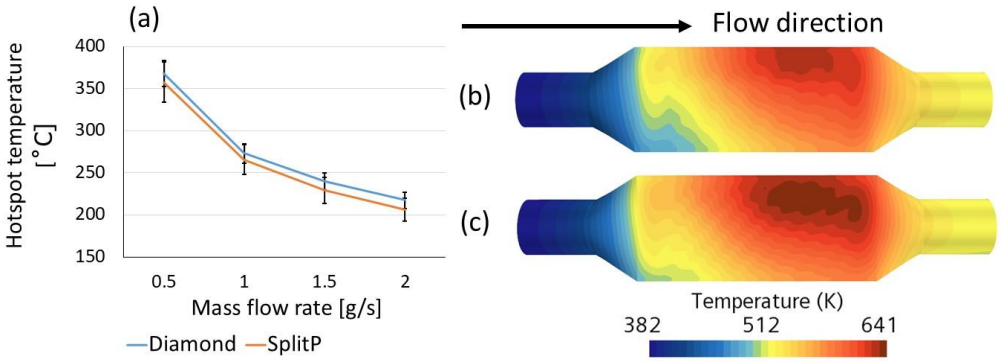

Figure 6. *Temperature map for mass flow rate of 0.5 g/s and heat flux level of 200 kW/m² for (a) SplitP and (b) Diamond lattices.*

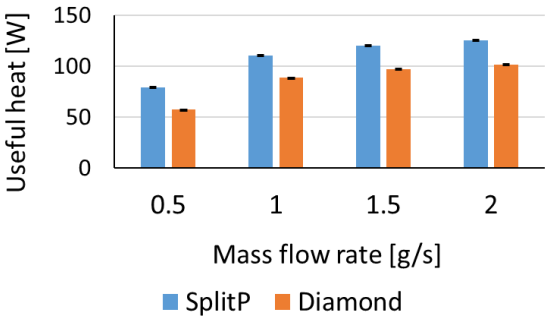

Figure 7. *The useful heat comparison between the two lattices obtained with Lag EB κ-ε*

5. Conclusion

In this study two high-temperature planar solar receivers equipped with SplitP, and Diamond lattices were studied numerically. The useful heat obtained from three different RANS turbulent models— Lag EB κ-ε, κ-ω SST (Menter), and Realizable κ-ε two-layer—were compared with experimental results, with Lag EB κ-ε and κ-ω SST (Menter) models showing the smallest error. All models underestimated the useful heat which could be attributed to rough surface of the samples which was not modelled in the simulations. To further validation of the model, the wall temperature increases of the location of TC_2 and TC_4 were compared with experimental data indicating the good consistency of the model. The receiver with SplitP lattice showed superior thermal performance with higher thermal efficiency, higher useful heat, and lower hotspot temperature. Also, the area with maximum temperature in SplitP was narrower than Diamond lattice.

Author contributions

A. Mortazavi: Methodology, Software, Validation, Formal analysis, Investigation, Data curation, Visualization, Writing – original draft. **H. Ebadi:** Methodology, Software, Validation, Investigation, Visualization, Writing – original draft. **C. Piatti:** Investigation, Resources, Software. **E. Gajetti:** Investigation, Resources. **L. Marocco:** Writing – review and editing, Supervision, Resources, Methodology, Conceptualization, funding acquisition. **L. Savoldi:** Writing – review and editing, Supervision, Resources, Methodology, Conceptualization.

Funding

The experimental work has received funding from the European Union's Horizon 2020 Research and Innovation Program under grant agreement n° 823802 (EU SFERA-III).

Competing interests

The authors declare that they have no competing interests.

Acknowledgement

We acknowledge the computational resources provided by hpc@polito, a project of Academic Computing at the Department of Control and Computer Engineering, Politecnico di Torino (http://hpc.polito.it).

References

[1] M. G. Gado, S. Ookawara, H. Hassa, "Utilization of triply periodic minimal surfaces for performance enhancement of adsorption cooling systems: Computational fluid dynamics analysis," Energy Conversion and Management, vol. 277, p. 116657, 2023, https://doi.org/10.1016/j.enconman.2023.116657

[2] J. Wang, K. Chen, M. Zeng, T. Ma, Q. Wang, Z. Cheng, "Investigation on flow and heat transfer in various channels based on triply periodic minimal surfaces (TPMS)," Energy Conversion and Management, p. 116955, 2023, https://doi.org/10.1016/j.enconman.2023.116955

[3] K. Dutkowski, M. Kruzel, K. Rokosz, "Review of the State-of-the-Art Uses of Minimal Surfaces in Heat Transfer," Energies, vol. 15, p. 7994, 2022, https://doi.org/10.3390/en15217994

[4] D. Xu, M. Lin, "Design controllable TPMS structures for solar thermal applications: A pore-scale vs. volume-averaged modeling approach," International Journal of Heat and Mass Transfer, vol. 201, p. 123625, 2023, https://doi.org/10.1016/j.ijheatmasstransfer.2022.123625

[5] L. Avila-Marin, J. Fernandez-Reche, S. Gianella, L. Ferrari, D. Sanchez-Señoran, "Experimental study of innovative periodic cellular structures as air volumetric absorbers," Renewable Energy, vol. 184, pp. 391-404, 2022, https://doi.org/10.1016/j.renene.2021.11.021

[6] Mortazavi , A. L. Ávila-Marín, H. Ebadi, E. Gajetti, C. Piatti, L. Marocco, L. Savoldi, "Experimental investigation of Triply Periodic Minimal Surfaces for high-temperature solar receivers," Case Studies in Thermal Engineering, vol. 60, 2024, https://doi.org/10.1016/j.csite.2024.104771

[7] J. Li, J. Gonzalez-Aguilar, C. Pérez-Rábago, H. Zeaiter, M. Romero, "Optical analysis of a hexagonal 42kWe high-flux solar simulator," Energy Proc. , vol. 57, pp. 590-596, 2014, https://doi.org/10.1016/j.egypro.2014.10.213

[8] F. Boydağ, "The optical properties of some steel surfaces with different surface preparations for high temperature use," Solar Energy Materials, vol. 13, pp. 185-195, 1986, https://doi.org/10.1016/0165-1633(86)90017-1

[9] M. Cantone, M. Cagnoli, J. F. Reche and L. Savoldi, "One-side heating test and modeling of tubular receivers equipped with turbulence promoters for solar tower applications," Applied Energy, vol. 115519, p. 277, 2020, https://doi.org/10.1016/j.apenergy.2020.11551